Analysis of Propeller-Hull Interaction Phenomena on a Self-Propelled Axisymmetric Body

(article starts on next page)

Analysis of Propeller-Hull Interaction Phenomena on a Self-Propelled Axisymmetric Body

Arash Eslamdoost[1], Jennie Andersson[1], Rickard Bensow[1], Robert Gustafsson[2], Marko Hyensjö[2]

[1]Department of Shipping and Marine Technology, Chalmers University of Technology, Gothenburg, Sweden
[2]Rolls-Royce Hydrodymanic Research Centre, Kristinehamn, Sweden

ABSTRACT

The Reynolds Transport theorem for energy is used to study propeller-hull interaction effects by analyzing different components of energy flux through a control volume around a self-propelled vessel. These components are the axial kinetic energy, the transversal kinetic energy, the turbulent kinetic energy, the internal energy and the pressure work. This energy balance approach is here used to study the influence of propeller diameter on the propulsive power. To this end, propellers of different diameters have been studied in behind condition. In order to keep the incoming wake into the propellers as simple as possible, an axi-symmetric hull shape is employed. The energy fluxes are calculated employing a RANS approach to solve the momentum transport and continuity equations together with the energy equation (the heat transfer equation in fluid). The latter equation is solved to compute the internal energy. The results show a minor difference on interaction effects. However, analyzing the energy flux components and their contribution to the total energy provides an extra tool for better understanding of the interaction effects.

Keywords

Propeller-hull interaction, self-propulsion, energy balance, control volume

1 INTRODUCTION

The interaction effects between propeller and hull are important design factors. The performance of the entire system can be improved noticeably by considering the interaction effects during the propeller and hull design process. These effects are most commonly described using a well-established terminology, including thrust deduction, wake fraction, propulsive efficiency etc. Such a description has an important drawback since it is based on experimental rather than theoretical considerations. This can imply limitations both in redesign and optimization of existing propulsion concepts. Limitations of the classical methods for analyzing the interaction effects are even more pronounced when distinctive designs with less understood physics are considered.

We believe that computational fluid dynamics (CFD) has reached a degree of maturity which can be used to extract more detail and precise data of the flow around self-propelled craft, even in full scale. Such information can aid us to understand the interaction effects deeper rather than through assessment of a few global values such as wake fraction and thrust deduction.

Several attempts have been made to develop methods and guidelines based on CFD or analytical approaches for analyzing the interaction effects. Dyne and Jonsson (1989) and Dyne (1995), by means of splitting a self-propelled system into a bare hull and an open-water propeller, proposed a method to study the propulsive efficiency based on wake losses and gains. This method is mostly derived based on potential flow assumptions, which implies that it is not correct to apply it for analyzing viscous flow simulation results. In order to achieve a better system efficiency, Dang et al. (2012, 2015) studied the dimensionless kinetic energy evaluated in the wake for two different applications. The method is easily applicable for analyzing CFD results. Although this approach does not take all the energy components into account, it has been used successfully for comparing the axial and transverse kinetic energy losses. Van Terwisga (2013) evaluated the propulsion power based on wake losses downstream of self-propelled hull. Similar to the marine sector, propulsor-hull interaction has been in focus of research in aircraft industry. For instance, Drela (2009) and Capitao-Patrrao et al. (2016) kept track of energy fluxes through control volumes which they used around their studied cases.

The objective of the current paper is to understand the interaction effects due to propeller diameter variation by applying a complete system energy balance approach. To this end, a series of propellers of different diameter are designed and used on a self-propelled axisymmetric body, the DARPA Suboff, (Haung et al. 1992). Based on the bare hull wake at the propeller plane, first, a wake adapted reference propeller was created. Then some other design variants with larger diameters were created. Due to the different propeller diameters, the mean wake is different for each of them which eventually results in different self-propulsion power. The system energy balance study enables us to look into details of the propeller-hull

interaction effects and better understand the total system performance.

2 CONTROL VOLUME ENERGY ANALYSIS

We can keep track of the total energy delivered to the system (propeller work) through the energy components and their conversion from one form to another. This can be done with the aid of the Reynolds Transport Theorem. This theorem states that for a steady state system, the change of any quantity (here total energy, E) plus the production of that quantity within a control volume enclosing a system is equal to the sum of the flux of that quantity over the surfaces of the control volume. A sample control volume around the case studies in this paper is shown in Figure 1.
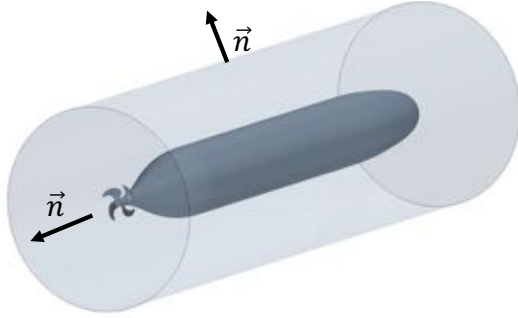

Figure 1. A sample cylindrical control volume around the axisymmetric body and the propeller.

In a steady state flow where no body force is acting on the system, the Reynolds Transport theorem for energy per unit mass e, for a control volume simplifies as follows,

$$\int_{CS} e\rho(\vec{u}\cdot\vec{n})\,dS = \int_{CS}(-p\cdot\vec{n}+\vec{\tau})\cdot\vec{u}\,dS, \qquad (1)$$

where the fluid velocity vector and density are denoted by $\vec{u}$ and ρ, respectively. The surfaces which enclose the control volume are denoted by CS with their unit normal vector, $\vec{n}$, pointing out of the control volume. The right-hand side is the integrand of force×velocity on control surfaces and represents the work done by the pressure and shear forces on the control volume. The pressure and the surface shear stress vector are shown by p and $\bar{\tau}$, respectively.

The right-hand side of Equation (1) can be split into the pressure and shear stress work acting on the material surfaces, CS_{MS} (hull and propeller), and on the virtual surfaces, CS_{VS} (outer enclosing surfaces), of the control volume. The former component for the test case used in this study is the propeller work,

$$P_D = 2\pi nQ, \qquad (2)$$

where n is the shaft revolution per second and Q is the shaft torque.

The force work surface integral (RHS of Equation (1)) on CS_{VS} can be simplified. Provided that the control surfaces are located far from the studied self-propelled object or normal to the local flow direction, we can neglect the shear

stresses acting on CS_{VS} and just consider the pressure force contribution.

In order to evaluate the energy distribution inside the control volume, e can be decomposed to four different components: (1) kinetic energy in the axial direction (2) kinetic energy in the transverse directions (3) turbulence kinetic energy and (4) internal energy. Since, the flow cannot penetrate CS_{MS}, LHS of Equation (1) simplifies to a surface integral just on CS_{VS}.

Considering the assumptions and divisions explained above, Equation (1) can be simplified as follows;

$$P_D = \int_{CS}\frac{1}{2}u_x^2\rho(\vec{u}\cdot\vec{n})\,dS + \int_{CS}\frac{1}{2}(u_r^2+u_\theta^2)\rho(\vec{u}\cdot\vec{n})\,dS$$
$$+ \int_{CS}k\rho(\vec{u}\cdot\vec{n})\,dS + \int_{CS}\hat{u}\rho(\vec{u}\cdot\vec{n})\,dS + \int_{CS}p(\vec{u}\cdot\vec{n})\,dS, \qquad (3)$$

where k is the turbulent kinetic energy and u_x, u_r and u_θ are the axial, the radial and the tangential velocity components, respectively.

The first four terms on the right-hand side are the axial kinetic energy, the transverse kinetic energy, the turbulent kinetic energy and the internal kinetic energy fluxes, respectively. The fifth term represents the work done by pressure forces on CS_{VS}. The internal energy change within the control volume (the fourth term on the RHS), can be obtained through,

$$\hat{u} = c_p T, \qquad (4)$$

where c_p is the specific heat of water and T is temperature.

In summary, the addressed energy balance method shows that the propeller shaft power of a self-propelled vessel is balanced with a set of different energy flux components through the surfaces of a deliberate control volume enclosing the system.

3 COMPUTATIONAL METHOD, DOMAIN AND MESH

We have employed the commercial CFD package STAR-CCM+, a finite volume method solver, in this study. The code solves the conservation equations for momentum, mass, turbulence quantities and temperature using a segregated solver based on the SIMPLE-algorithm. A 2nd order upwind discretization scheme in space was used. We have also solved the energy equation, to be able to measure the dissipation of kinetic energy and turbulent kinetic energy in the form of temperature (Equation (4)). Since the wake into the propeller is circumferentially symmetric, the Moving Reference Frame (MRF) technique was used to model propeller rotation. The turbulence was modeled using a RANS approach and the k-ω SST model. All the aforementioned equations were solved employing a steady-state solver.

The propeller revolution rate was changed until the thrust and the resistance of the propeller and hull were in balance.

This was an iterative process in which the propeller revolution rate was part of the solution.

The computational domain is shown in Figure 2. As seen in this figure, the DARPA Suboff model is L = 4.356 m long and has a maximum dimeter of 0.508 m. The inlet boundary with a constant inlet velocity was located 4L in front of the hull. The inlet velocity was set to 2.767 m/s, equivalent to Re = 1.2×10^7(fresh water as the operating medium and L as the reference length). The outlet boundary was placed 10L downstream of the hull. A constant pressure boundary condition was used on this boundary. A cylinder with a diameter of D = 7L was used as the surrounding boundary and a symmetry boundary condition was imposed on it.

Different mesh types have been used in different part of the computational domain. Trimmed hexahedral grids were used around the hull as well in the far field region but the computational grid for the propeller domain consists of polyhedral cells due to the complex geometry with high curvatures in this region. Prism layers along walls are used to create the boundary layer mesh. Due to dissimilar boundary layer thickness on the hull and the propeller blades, different prism layer thicknesses are used for each of these surfaces and thus the number of prism layers were adjusted accordingly. The number of prism layers were set to 35 and 20 on the hull and propeller blades, respectively. In order to resolve the boundary layer down to the wall, the near wall cell's height was adjusted to obtain $y^+ \approx 1$. The grid distribution inside the computational domain as well as the hull and propeller surface is shown in Figure 3. As seen in this figure, the finest mesh region is around the propeller and the mesh gradually becomes coarser further away from the propeller and hull. The total number of cells is 11 million cells of which about 1 million of that is dedicated to the propeller region.

4 PROPELLER DESIGN METHOD

A series of propellers of different diameter were designed to propel the DARPA Suboff. Based on the bare hull nominal wake at the propeller plane, first, a wake adapted reference propeller was created. Then some other design variants with larger diameters were created. Figure 4 shows the bare hull wake distribution at the propeller plane. The vertical axis shows the non-dimensional radial distance from the propeller center. R_0 is the maximum radius of the axisymmetric body and U_0 is the undisturbed free-stream velocity. The wake presented in this figure was used in the design process of the propellers.
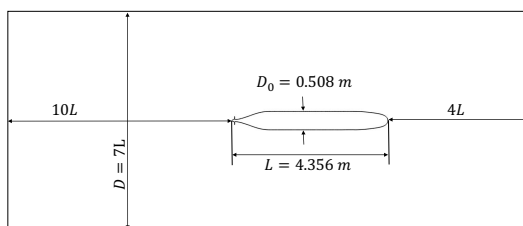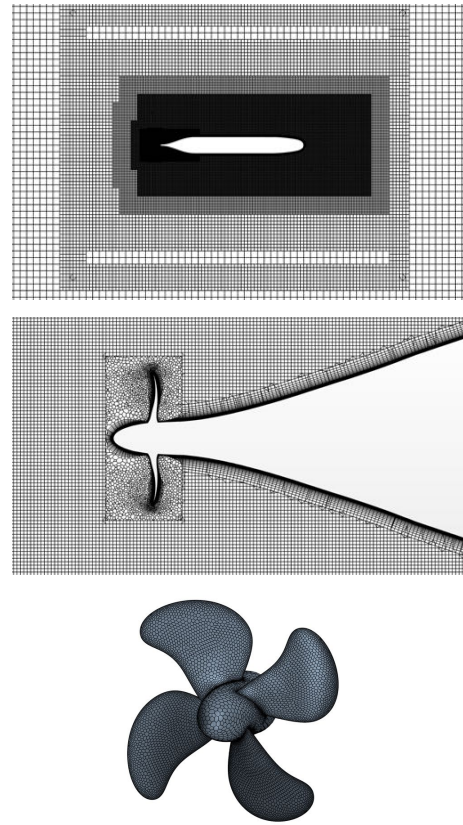

Figure 2. Computational domain.

Figure 3. Grid distribution (a) near field region, (b) aft part boundary layer prism layer and propeller region mesh and (c) propeller surface mesh.
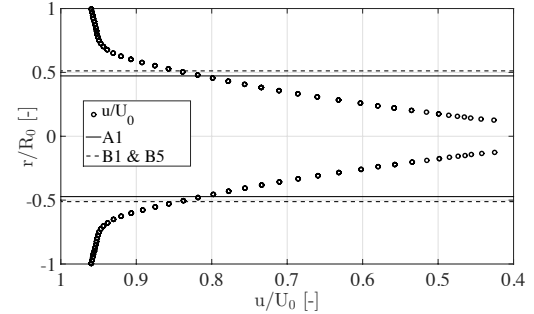

Figure 4. Bare hull wake at the propeller section. The A1, B1 and B5 vertical lines shows the radii of different designs.

The propellers are designed with the same tools, standard distributions of chord length, skew, rake, load distribution and set of requirements to have a common design philosophy through all propeller designs. The shaft speed for each propeller is calculated to yield optimum efficiency following standard series analysis. The blade area of the baseline propeller, A1, with a diameter of 0.12 m was calculated with a standard cavitation margin against back side bubble cavitation. Then a larger propeller, B1, with a diameter of 0.13 m (8.3% larger than A1) was created with the same cavitation margin as A1. This larger propeller, at the optimum shaft speed, has a higher open water efficiency than A1. A further variant of the larger propeller was created by lowering its efficiency in self-propulsion, down to the efficiency of A1 in self-propulsion, through

increasing the blade area. This new variant is called B5 throughout this paper. Figure 5 shows these different designs. Among these designs B1 has the best self-propulsion efficiency. A1 and B5 have the same self-propulsion efficiency which is lower than that of B1. The reason for introducing B5 beside B1 is to provide a fair condition to compare a larger propeller with the reference propeller, A1,
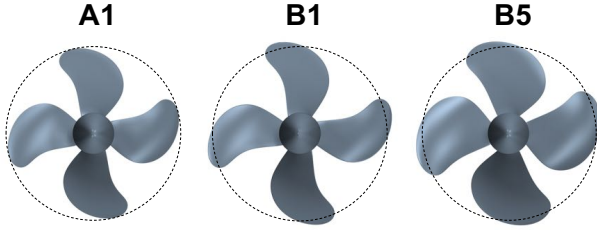

Figure 5. Different propeller designs.

5 RESULTS AND DISCUSSION

Two control volumes with different sizes are employed in the process of post processing the results. The first control volume is a cylinder which only surrounds the propeller. The other control volume is much larger and contains the entire propeller-hull system. Figure 6 depicts both of the control volumes. The size and placing of the aforementioned control volumes are the same for all three self-propulsion cases.

Based on the theory presented in Section 2, two methods were used for computing the power consumption in self-propulsion for each propeller design. The first method was an explicit approach through direct computation of the propeller torque (Equation (2)) and the second method was based on the control volume energy balance method (Equation (3)). The latter method was evaluated on both CV1 and CV2. Table 1, shows the result of these different methods. The power computed from the energy balance method for CV1 and CV2 are denoted as P_{CV1} and P_{CV2} in this table. The power obtained through the energy balance on CV1 deviates less than 0.7% from the explicitly computed power (P_{CV1} error $= 100 \times (P_{CV1} - P)/P$, less than 0.7%), however, the deviation becomes slightly larger on CV2 (P_{CV2} error, less than 1.1%). The P_{CV2} errors are related to the larger numerical errors associated with the coarser mesh in the far field region where the control surfaces of CV2 are placed. The absolute energy flux on each of the surfaces of the control volume are much larger than the sum (P_{CV2}) which makes the results very sensitive to the accuracy of the computed surface fluxes, hence the control volume surface mesh quality.
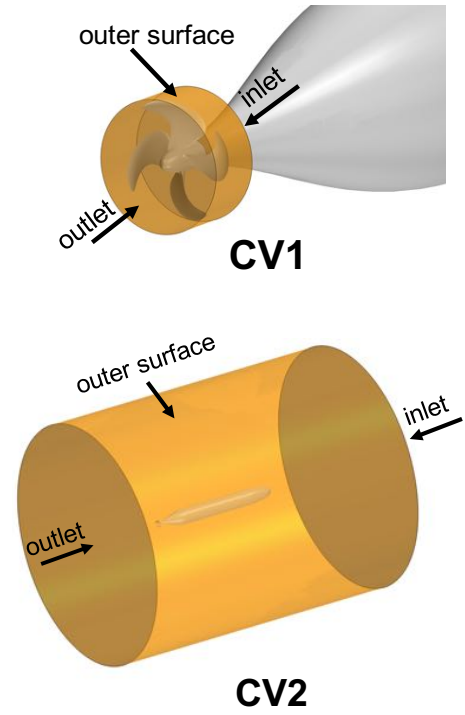

Figure 6. Two different control volumes (top) only containing the propeller, CV1, and (bottom) containing both the propeller and hull, CV2.

Another interesting finding is the sensitivity of the power computed from the energy balance method to the shear stress on the control surfaces. As indicated in the theory section, the contribution of the shear stress work to the energy fluxes through the control volume has been neglected in this study. This could be a reasonable assumption for CV2, since the control surfaces are located far from the propeller and hull where no large velocity gradients (normal to the control surfaces) can exist.

However, this might not be the case for CV1 which is associated with large velocity gradients close to its control surfaces. Since the CV1 size is the same for all the computations, the clearance between the propeller B1/B5 tip and the outer surface of the control volume is much smaller than that of A1. As a result, the velocity gradient normal to the cylindrical control surface becomes larger for B1 and B5 and thus the contribution of shear stress to the energy flux through this surface might not be negligible. The P_{CV1} error in Table 1 confirms this statement. Due to the larger A1 tip clearance in comparison to B1 and B5, the computed P_{CV1} is much closer to the explicitly computed P (0.03% deviation).

Table 1. Powers computed from different methods.

	n	T_{net}	Q	P	P_{CV1}	P_{CV1} Error	P_{CV2}	P_{CV2} Error
	[rps]	[N]	[N.m]	[W]	[W]	[%]	[W]	[%]
A1	10.42	78.70	3.60	235.70	235.77	0.03	233.18	-1.07
B1	9.05	78.34	4.05	230.29	231.77	0.64	227.96	-1.01
B5	8.18	79.25	4.62	237.45	239.10	0.69	235.74	-0.72

The distribution of the energy flux components through CV2 for A1, B1 and B5 is shown in Figure 7. The energy components in this bar chart are the ones which were introduced in Equation (3). The sum of these components is equal to P_{CV2}, presented in Table 1. The most dominant component in this figure is the internal energy. Far away downstream of the self-propelled system, all the energy components turn into internal energy or simply dissipate in the form of heat. Since the control surfaces of CV2 are placed in far field, the internal energy flux will be the dominant component. Although the application of such a large control volume shows the possibility of obtaining energy balance even through CV2, the diminishing energy components cannot provide further information to compare the interaction effects between the distinctive designs. Thus, it would be more beneficial to use as small control volumes as possible around the studied case. The results of the system energy balance using a much smaller control volume, CV1, are presented in the following section.
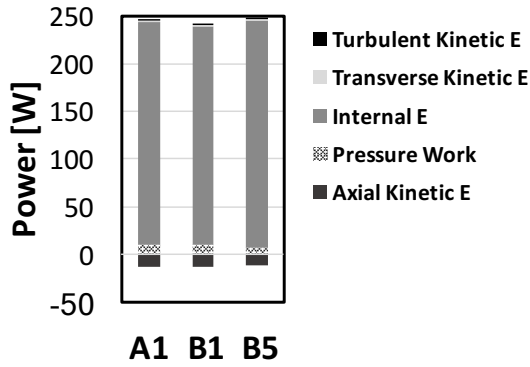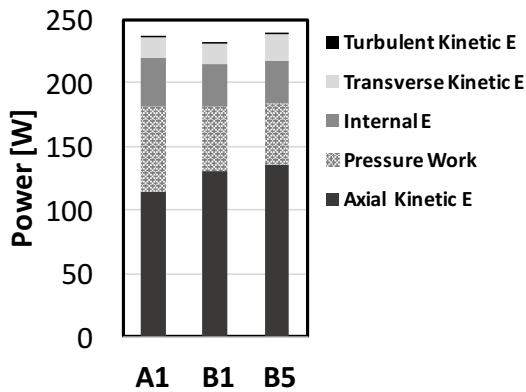

Figure 7. Energy flux components through CV2.

Figure 8. Energy flux components through CV1.

The distribution of the energy flux components through CV2 for A1, B1 and B5 is shown in Figure 8. The axial kinetic energy flux and the pressure work on CV1 are proportions of the useful energy components which have not been converted to internal loss yet. The sum of these two components is almost constant for the different propeller designs, which indicates similar propeller-hull interaction effects for all the three designs. We can support this idea by the almost identical net thrust requirement for A1, B1 and B5, reported in Table 1. Comparison of the pressure distribution on the aft-part of the hull for the different propeller designs also confirms this finding. Figure 9 shows the pressure coefficient distribution on the aft-part of the bare hull as well as the self-propelled cases. The bare hull pressure coefficient shows a good agreement with the measured data (circles). As expected, the propellers induce suction on the aft-part of the hull and the self-propulsion tail pressure distribution starts to deviate from the bare hull pressure (noticeable after $X/L = 0.87$). However, the propeller induced pressure is so similar for the different designs that one can barely detect any difference between them. In summary, all these evidences show that the thrust deduction is the same for all the three propellers, despite their different diameters and operating conditions.
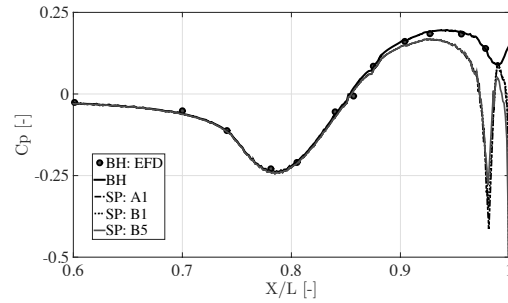

Figure 9. Aft-part pressure coefficient for the bare hull and self-propelled hull with three different propeller designs.

The axial kinetic energy flux and the pressure work distribution on the outlet of CV1 is shown in Figure 10. The axial kinetic energy flux through this section is the lowest at the center due to the hub wake. Moreover, because of the low-pressure region inside the hub vortex, the pressure work has its minimum value at the center. For the larger propellers, in comparison with the reference propeller, a slightly larger ring shaped region of high axial kinetic energy flux can be seen around the center. This can be related to the larger axial kinetic energy flux through CV1 for B1 and B5 in comparison to A1, as reported in Figure 8. However, the decreased pressure work of the larger propellers cannot be easily seen just by analyzing the outlet section of CV1. Actually, a better picture of the energy flux components can be obtained through comparison of all the surfaces of the control volume and not only the outlet boundary. Performing such an analysis shows that the deviation of the pressure work acting on the suction side boundary of CV1 is much dominant than the outlet or outer boundaries' contribution to the total pressure work between the small and the larger propellers. The inlet pressure work of CV1 is much higher for the larger propellers than A1 (with opposite sign respect to the outlet) and thus the surface integrals of the pressure work on all surfaces of CV1 for B1 and B5 are smaller than that of A1, as seen in Figure 8.
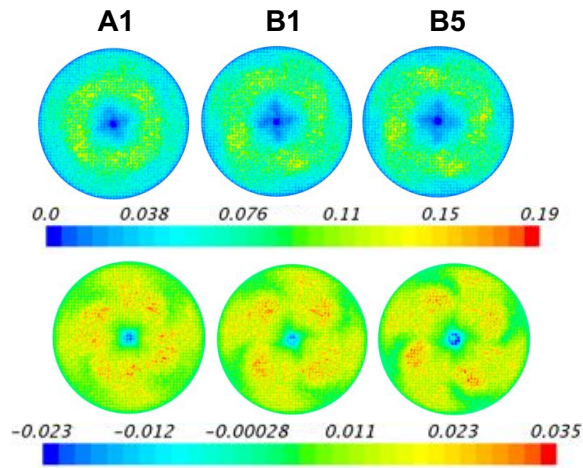
Figure 10. Distribution of the useful energy components for different propeller designs just behind the propeller (top) axial kinetic energy and (bottom) pressure work.

The transverse kinetic energy, the internal energy and the turbulent kinetic energy are not doing useful work and can be considered as loss components. According to Figure 8, the modelled turbulent kinetic energy has a minor contribution to the total energy and can be neglected. Since the sum of the axial kinetic energy and the pressure work are almost the same for all the three designs, it is only the energy loss components which determine the overall efficiencies of the propellers.

Among the propellers, the same amount of energy is converted to internal energy (heat) for B1 and B5, but the internal energy contribution for A1 is 15% larger. The faster rotational speed of A1 could create a flow where there is larger energy dissipation in the form of heat, which means a larger internal energy in the flow (see Table 1). B5 rotates slower than B1, but its larger blade area could be compensating for the lower rotational rate and thus the same internal energy. The distribution of the internal energy flux through CV1 outlet is shown in Figure 11. The internal energy flux through this surface is almost the same for B1 and B5 whereas the flux of A1 is slightly higher, especially in the center.

The transverse kinetic energy in Figure 8 is the last loss component to be discussed. Almost the same amount of energy is converted to the transvers kinetic energy for A1 and B1 whereas the value is about 30% larger for B5. This loss component is due to the non-axial velocity components through the control volume surfaces. The transverse kinetic energy flux distribution on the outlet control surface of CV1 is shown in Figure 11. As seen here, the distribution of this energy flux component is very similar for A1 and B1, however a more prominent transverse energy flux values can be detected in the core of B5. This reveals the existence of a stronger hub vortex for B5 which increases the transverse kinetic energy loss in comparison to A1 and B1. Vortical structures in the flow can represent the transvers energy components. These structures increase the non-axial velocity components which consequently increase the transvers kinetic energy

contribution to the total energy. The Q-criterion is used to visualize these structure in Figure 12. A constant positive Q-criterion is used to extract the iso-surfaces plotted in this figure. The extent of vortical structures are the largest for B5 and the smallest for A1, which is well aligned with the computed transverse kinetic energy flux components presented in Figure 8.
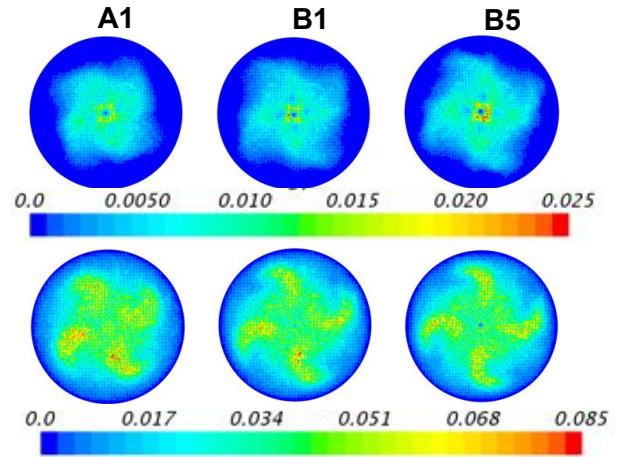

Figure 11. Distribution of the loss components for different propeller designs just behind the propeller (top) transverse kinetic energy and (bottom) internal energy.
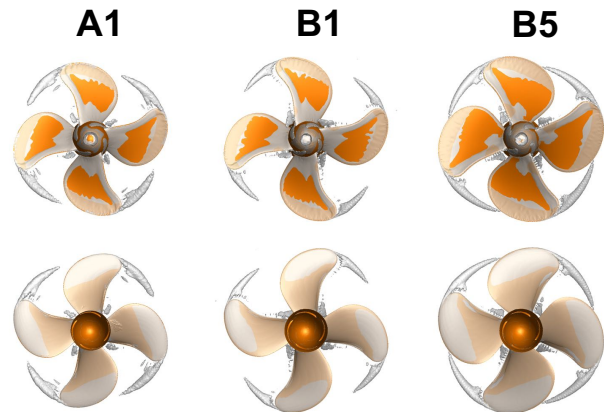

Figure 12. Q-criterion iso-surface on the propellers; Pressure side (top) and suction side (bottom).

CONCLUSIONS

As shown in this paper, analysis of the energy flux components through a control volume around a self-propelled hull provides more detailed information on how the propeller work is converted to different forms of energy. It was shown that all energy is converted to internal energy in far field downstream of the propeller. Thus, in order to see a clearer division between all the energy components, we suggest to set up a small control volume around the propeller rather than a large control volume which extends to far field downstream of the propeller. The loss component in the form of internal energy will not be

dominant for smaller control volumes and instead useful information on the distribution between other energy components, the axial kinetic energy, the pressure work, and the transversal kinetic energy, will be discernable. This makes it more convenient to compare different propeller designs with each other.

Among the three propellers studied in this paper, the larger diameter propeller which was designed with the same design philosophy and cavitation margin as the reference propeller yields the lowest self-propulsion power demand (2.3% lower power). The analysis of the energy fluxes through a small control volume around these two propellers (A1 and B1) reveals that the sum of the useful energy components (axial kinetic energy and the pressure work) are almost the same for these two designs. This could be tied into the same generated net thrust generated by these propellers. Thus, one can conclude that the main reason for the better performance of the larger propeller is because of lesser accumulated energy loss components for this design.

Taking a closer look at the individual loss components also reveals that both the propellers attain the same level of transversal kinetic loss component and thus the only term which makes the larger propeller to perform better is its lower internal energy loss (about 13% lower). The main reason for the lower internal energy loss, or less heat generation, of the larger propeller could be its lower revolution rate (about 13% lower) and thus generation of less turbulent structures in the flow which eventually dissipate in the form of heat.

REFERENCES

Capitao-Patrrao, A. et al., 2016. Proc. of ASME Turbo Expo. In *Wake and loss analysis for a double bladed swept propeller*. Seoul, South Korea.

Dang, J., Dong, G. and Chen, H., 2012. An exploratory study on the working principles of energy saving devices (ESDS) – PIV, CFD investigations and ESD design guidelines. In *OMAE2012*. Rio de Janeiro, Brazil.

Dang, J., Hao, C., Rueda, L. and W.H., 2015. Integrated Design of Asymmetric Aftbody and Propeller for an Aframax Tanker to Maximize Energy Efficiency. In *4th International Symposium on Marine Propulsors*. Austin, USA.

Drela, M., 2009. Power balance in aerodynamic flows. *AIAA Journal*, 47(7), pp.1761–1771.

Dyne, G., 1995. The principles of propulsion optimization. In *Trans. RINA 137*. London, United.

Dyne, G. & Jonsson, L.., 1989. A Method for Analysing and Simulating Propulsion Systems. In *International Symposium on Practical Design of Ships and Mobile Units (PRADS), 4th*. Bulgarian Ship Hydrodynamics Centre, Varna, Bulgaria.

Haung, T. et al., 1992. Measurements of Flows Over an Axisymmetric Body With Various Appendages in a Wind Tunnel: the DARPA Suboff Experimental Program. In *19th Symposium on Naval Hydrodynamics*. Seoul, Korea, pp. 321–346.

Terwisga, T., 2013. On the working principles of Energy Saving Devices. In *3rd International Symposium on Marine Propulsors*. Launceston, Australia.

DISCUSSION

Question from Tom van Terwisga
It is interesting to see that you found a relatively large amount of thermal energy flux, which possibly is the kinetic turbulent energy dissipated into heat. We did a similar investigation for a propeller in open water (Schuling et al. 2016) where we only included the turbulent kinetic energy flux (and no heat flux) and found a discrepancy in our energy analysis of some 2-3%. This was attributed to numerical dissipation. Could you comment on the role of numerical dissipation in your internal energy flux?

Author's closure
We believe that the numerical dissipation contributed to the internal energy fluxes through the control volume. This can be evaluated through a systematic mesh dependence study, which was not carried out in this study. However, the results of applying our method to a propeller in open water shows a dependence of the energy fluxes, including the internal energy flux, on the grid refinement level. Finer grids are expected to have smaller numerical dissipation which could be confirmed by the lower internal energy flux level. According to the systematic grid refinement study in open water, we found a variation of the internal energy flux within just a couple of percent.

Moreover, the control volume size has an impact on the energy fluxes. We have studied two different control volume sizes in this study. The accumulated energy fluxes obtained from the smaller control volume shows a better match with the shaft delivered power in comparison to the larger control volume (see Table (1)). The numerical dissipation increases by an increasing control volume size which consequently contributes to the increment of the internal energy fluxes.

Question from Tom van Terwisga
I would expect a significant difference in the sum of axial kinetic energy loss and the pressure work between the smaller propeller and the two bigger propellers, analogous

to the differences in ideal efficiency. But I do not see that in your energy fluxes. Could you comment on this?

Author's closure
The sum of axial kinetic energy flux and the pressure work represent the required thrust to propel the system as well as certain amount of losses (mixing losses). Since the propellers' thrust are almost the same (same thrust deduction fraction, see Figure 9), this sum is almost the same for all the propellers. Propeller B1, which has a larger diameter in comparison to A1, has been designed with the same constrains as A1. As a direct result, B1 has a higher efficiency than A1. Figure 8 shows the energy flux components for these two propellers. As stated above, since the thrust requirements are the same for these two propellers, the sum of the axial kinetic energy flux and the pressure work are also the same. However, the sum of the internal, transverse and turbulent kinetic energy fluxes, which represent the losses, are smaller for B1. Provided that the propeller efficiency is the ratio of the useful energy flux components to the loss components, the efficiency of B1 will be larger than A1, analogous to the ideal efficiencies. This statement holds for propeller B5 as well. As seen in Figure 8, the sum of axial kinetic energy and the pressure work is slightly larger than A1. On the other hand, sum of the losses is larger for B5 in comparison to A1. But interestingly, the ratio of the useful energy flux components to the unprofitable energy flux components is almost the same as for A1, confirming that these propellers have the same efficiencies.